Phys Chem Minerals (2001) 28: 557–571

ORIGINAL PAPER

J. D. Lawlis · Y.-H. Zhao · S. Karato

High-temperature creep in a Ni_2GeO_4: a contribution to creep systematics in spinel

Received: 18 June 2000 / Accepted: 3 April 2001

Abstract High-temperature creep behavior in Ni_2GeO_4 spinel was investigated using synthetic polycrystalline aggregates with average grain sizes ranging from submicron to 7.4 microns. Cylindrical samples were deformed at constant load in a gas-medium apparatus at temperatures ranging from 1223 to 1523 K and stresses ranging from 40 to 320 MPa. Two deformation mechanisms were identified, characterized by the following flow laws:

$$\dot{\varepsilon} = 10^{2.95\pm0.15}\sigma^{2.9\pm0.1}\exp\left(\frac{416 \pm 16\ \text{kJ mol}^{-1}}{RT}\right)$$

$$\dot{\varepsilon} = 10^{5.53\pm0.21}\frac{\sigma^{1.0\pm0.2}}{d^{3.0\pm0.2}}\exp\left(-\frac{281 \pm 11\ \text{kJ mol}^{-1}}{RT}\right),$$

where σ is in MPa, d is in μm and T is in Kelvin. These flow laws suggest that deformation was accommodated by dislocation creep and grain-boundary diffusion (Coble) creep, respectively. A comparison with other spinels shows that an isomechanical group can be defined for spinels although some differences between normal and inverse spinels can be identified. When creep data for olivine and spinel are normalized and extrapolated to Earth-like conditions, spinel (ringwoodite) has a strength similar to olivine in the dislocation creep regime and is considerably stronger than olivine in the diffusion creep regime at coarse grain size. However, when grain-size reduction occurs, spinel can become weaker than olivine due to its high grain-size sensitivity (Coble creep behavior). Analysis of normalized diffusion creep data for olivine and spinel indicate that spinel is weaker than olivine at grain sizes less than 2 μm.

Key words Spinel · Olivine · Germanate · Dislocation creep · Diffusion creep · Coble creep

J. D. Lawlis · S. Karato (✉)
Department of Geology and Geophysics,
University of Minnesota, Minneapolis,
Minnesota 55455, USA
Fax: +1-612-625-3819
e-mail: karato@karato.email.umn.edu

Y.-H. Zhao
Department of Geophysics, Peking University,
Beijing 100871, PR China

Introduction

Understanding the creep behavior of high-pressure minerals is critical to the understanding of the dynamics of the Earth's interior. Direct mechanical tests under deep mantle conditions remain difficult, however, and are limited to stress-relaxation tests (e.g., Karato and Rubie 1997). Under these circumstances, the use of analogue materials is a useful strategy to understand better the rheology of the Earth's deep interior (e.g., Frost and Ashby 1982; Karato 1989). This paper presents results of such a study on spinel, a major constituent in Earth's deep transition zone (~520 to ~660 km depth).

Systematic comparisons of the creep properties of many isostructural materials have been made in the past 20 years, including the oxide, garnet, and olivine families (Bretheau et al. 1979; Karato 1989; Karato et al. 1995). The results of these studies indicate that an isomechanical class can be defined for materials with the same structure but different chemistry, for which the type and strength of slip systems are similar. Materials within an isomechanical class are characterized by having similar nondimensional creep parameters (e.g., Q/RT_m and $\Omega G/kT_m$, where Q is the activation energy for creep, Ω is the atomic volume, G is the shear modulus and T_m is the melting temperature). Normalization provides a means for comparing materials with different melting temperatures and shear moduli under similar conditions. There is often a good correlation between the strengths of isostructural materials when they are compared under the same normalized conditions. Exceptions to this classification can usually be explained by factors relating

to the size and charge of the cations, stacking fault energies, or point-defect chemistry.

Germanates have long been regarded as suitable analogues for silicates based on analyses of common slip systems and crystal chemistry systematics (Ringwood 1970; Navrotsky 1967, 1973, 1977; Navrotsky and Hughes 1976; Vaughan and Coe 1981; Green and Burnley 1989; Dupas-Bruzek et al. 1998). In particular, magnesium germanate has been widely studied, not only because its composition is similar to that of mantle materials, but because it features an olivine-to-spinel transformation that can be produced at pressures under 2 GPa. This makes it ideally suited for investigation using a standard solid-medium deformation apparatus. Although compositions other than Mg_2GeO_4 have been investigated, mainly from the standpoint of determining the conditions of phase transformation, there has been no systematic investigation of the deformation behavior of any member of the germanate family other than magnesium germanate.

Furthermore, most studies (e.g., Vaughan and Coe 1981; Dupas-Bruzek et al. 1998) have aimed at establishing similarities between the slip systems of germanates and silicates, but have neglected to compare their normalized creep strengths. In part, this is due to a paucity of creep data for spinels containing tetrahedral cations (II–IV spinels), particularly silicate spinel, for which there are no creep data. It is not sufficient, however, to simply compare dislocation microstructures and slip systems of silicates and germanates to prove the usefulness of germanate spinel as a rheological analogue. We must demonstrate that spinels form an isomechanical class, so that creep data from germanate analogues can be used to predict the strength of silicate spinel in the Earth.

Creep experiments in a gas-medium apparatus are limited to minerals or rocks that are stable within the upper 10 km. It is impossible, therefore, to perform experiments on Mg_2GeO_4 spinel in a gas apparatus, since the spinel phase is not stable. By incorporating transition metal cations such as iron or nickel, it is possible to stabilize spinel at 1 atm pressure. We can perform mechanical tests in the dislocation and diffusion creep regimes by controlling the grain size, temperature, and differential stress. These transition-metal germanates are also relevant to the transition zone of the Earth, where transition-metal ions are thought to make up over 10% of the octahedral sites (Ringwood 1970).

Experimental procedure

Sample preparation

Powders of nickel germanate spinel (Ni_2GeO_4) were synthesized by reacting fine-grained (< 1 μm) powders of lab-grade NiO and GeO_2 (99.998% purity) in a 1-atm furnace. The reaction was conducted in two stages to prevent the initial melting of germania. The mixture was first heated at 1323 K for 18 h and then annealed at 1473 K for 34 h. All syntheses were performed in an Ar–10.4% CO_2 environment using an alumina boat covered with Ni foil. At first, powders of NiO and GeO_2 were mixed in a stoichiometric 2:1 ratio, cold-pressed, and reacted according to the above procedure. We found, however, that the resulting powders contained substantial amounts of NiO, due to the evaporation of germania occurring during the synthesis. When powders were mixed in a $2NiO:1.1GeO_2$ molar ratio, the rate of germania evaporation was slow enough to allow most NiO to react before evaporation was complete. The reaction product was light green in color and had the spinel structure. No noticeable traces of NiO or GeO_2 were found using X-ray diffraction (XRD) analysis.

Powders were ground in a mortar and pestle to < 1 μm and subsequently cold-pressed in an Ni can (11.5 mm OD, 30 mm length) at a differential stress of 200 MPa. The cold-pressed samples were then placed in a vacuum oven at 413 K for 1 day to remove adsorbed water on the surfaces of the grains. Samples were densified by hot-isostatic pressing (HIP) at a confining pressure of 300 MPa and temperatures ranging from 1173 to 1573 K in a gas-medium apparatus. We found that temperatures between 1373 and 1473 K were ideal for HIPing nickel germanate. At temperatures below 1273 K, powders were poorly densified and contained porosities of several percent, while at temperatures higher than 1523 K grain growth was abnormal, yielding a binormal grain-size distribution. Sample density was measured using the Archimedean method of weighing a sample in water and in air, and apparent porosity was calculated using the theoretical density of nickel germanate spinel ($\rho = 6{,}026$ kg m^{-3}). Despite our best efforts, it was difficult to achieve porosities less than 2%. All creep experiments were performed on samples containing 2–2.5% porosity.

A 1-mm section was cut from the end of the hot-pressed sample for grain-size measurement. Ordinarily, these sections would be polished to <1 μm and etched so that the grain shape can be clearly distinguished. This procedure was not used, however, because nickel germanate does not dissolve easily in acid. We tried to etch samples using several acids ranging from boiling HNO_3, HPO_4, HCl, HF vapor etch, HF immersion, and various combinations of the above, with no noticeable success. Finally, we were able to observe the grain boundaries by cracking open samples that had been heated to 1273 K and quenched. In this procedure, a fresh fracture surface was created using a hammer and a hardened steel implement with a sharp tip.

Deformation procedure

Samples were jacketed in either an Ni or Cu sleeve to buffer the oxygen fugacity (f_{O_2}) at either Ni/NiO or Cu/CuO. The inside of the Ni sleeves was coated with a slurry of predried NiO powder and ethanol and allowed to dry in a vacuum oven overnight. Sleeves of Cu were oxidized by heating in air so that a ~100-μm oxide layer was formed. In both cases, the oxide layer was sufficiently thick to buffer the oxygen fugacity. In addition, when the Cu sleeve was peeled away from the sample after an experiment, the metal remained discolored, suggesting the presence of an oxide film. The ends of the sample were polished flat and parallel before recording the length and cross-sectional area for strain and stress calculations. Alumina pistons were used to transmit the load, and contained a hole along the central axis. A thermocouple could be positioned at some distance from the sample so that the sample temperature could be monitored during the experiment. The temperature profile was calibrated prior to the experiment using a dummy sample and showed temperature variations of 1–2 °C across the 4-cm hot zone. For full details of the experimental assembly including diagrams see Paterson (1990).

Deformation experiments were conducted at 300 ± 5 MPa confining pressure in a servo-controlled gas-medium Paterson deformation apparatus. The apparatus is equipped with a capacitance-type internal load cell, yielding stress measurements accurate to ± 2 MPa. Stress-stepping experiments, in which samples were deformed at constant load in 1–2% strain increments, were performed on the majority of samples. Figure 1 shows a plot of strain versus time data for a typical experiment where deformation conditions (stress, temperature) were duplicated at the beginning and end of the deformation experiment. The good agreement between

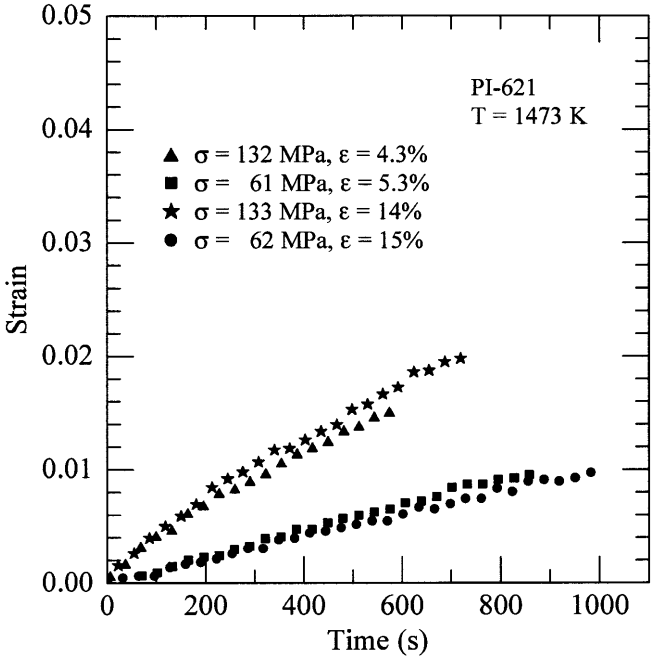

Fig. 1 Strain versus time data for a typical deformation experiment. Similar deformation conditions were applied at the beginning and end of the experiment to test for the presence of strain hardening. In this example, strain rates were virtually identical for two separate stresses, indicating that deformation is steady state with little to no strain hardening

the creep rates for these tests demonstrates that deformation was steady state and that little to no strain-hardening was observed up to 18% strain.

In their initial format, creep data exist as position versus time and load versus time files. The strain rate is calculated by taking the slope of the position versus time data and dividing by the instantaneous length (calculated from the position change during each creep test). Typical strain rates varied between 1×10^{-4} and 1×10^{-6} s^{-1} and had reached steady state by about 1% strain. We calculated differential stress by dividing the load by the instantaneous cross-sectional area of the sample. Differential stresses were typically between 40 and 300 MPa. Creep data for all experiments are shown in Table 1. They are shown sequentially, following the order in which each data point was collected.

At the end of the experiment, the load was removed and the temperature was dropped at a rate of 1 K s^{-1}. Upon removal of the sample assembly, the jacket was dissolved in aqua regia (nitric and hydrochloric acid). A 1-mm slice was cut from the deformed sample for grain-size analysis. We calculated sample porosity after deformation using the Archimedean method. In most cases the porosity did not change during the experiment except when the sample was deformed at temperatures above 1523 K, where the porosity increased slightly.

We used nickel jackets for all hot presses and most deformation experiments. These jackets do not react with Ni_2GeO_4 and they buffer the oxygen fugacity (f_{O_2}) of the sample at Ni/NiO. Samples that were jacketed by copper were noticeably darker in color (dark green). The reaction layer must be small (< 0.5 μm), however, as we were unable to detect copper in the interior of the sample using microprobe analysis.

Microstructural observations

Grain size was estimated by analyzing the fracture surfaces of deformed samples. More than 200 grains were traced from SEM micrographs for each sample. The traced images were analyzed using an NIH image analysis program, and grain sizes were calculated by assuming that grains were approximately spherical and that the area for each grain could be approximated by $\pi(kr)^2$, where r is the grain radius and k is a geometrical constant. We use $k = 1.22$, which assumes that spheres are sectioned randomly. This should be a reasonable approximation if underlying grains are partially obstructed by those on the surface. In the event that the correction factor k deviates from the random case, our grain-size analysis is still internally consistent and does not affect the determination of the grain-size exponent. Figure 2a shows an SEM image of a fractured surface of a typical hot-pressed nickel germanate sample. Grains are equant and have a grain-size distribution that is approximately log normal. The average grain size and distribution for this sample are shown in Fig. 2b. The reported average grain size for every sample is the logarithmic average.

Experimental results

The transition between the dislocation and diffusion creep regimes was located by performing a series of stress-stepping tests at constant temperature on a sample with a grain size of 7.4 μm. At low differential stress, the creep rate varied linearly with stress (diffusion creep behavior), while at higher stress the creep rate varied with the power of the stress (dislocation creep behavior). An example of this behavior is illustrated in Fig. 3a. Experiments were then performed in each region by varying the grain size and differential stress accordingly.

The creep rate is a function of temperature, stress, oxygen fugacity, and grain size. For the majority of deformation tests, we determined the creep rate as a function of one variable, holding all other variables constant. In this manner, creep parameters were determined independently for each variable. We prefer this technique, as opposed to one that uses multiple linear regression, because it provides a more accurate estimate of the error associated with each creep parameter. It was not always possible to hold all variables constant, such as when grain growth occurred during the course of an experiment. In these cases, creep data were corrected for the change in grain size, using a procedure that will be presented in a later section.

Experiments in the dislocation creep regime

Two deformation experiments were performed on samples with a grain size of 7.4 μm. In the first experiment, the temperature was held constant while the stress was varied. When the log creep rate is plotted against log stress, the stress exponent n can be determined. Figure 3a shows a plot of creep data from experiment PI–604, in which the stress exponent changes from $n \sim 1$ at lower stress to $n = 2.9 \pm 0.1$ at higher stress. The change in slope occurred at $\sigma = 200$ MPa at 1423 K and, at $\sigma = 180$ MPa at 1473 K.

The second deformation experiment was performed at constant stress while the temperature was varied. This type of experiment is useful for determining the activation energy for dislocation creep. Creep rates were

determined at 220 and 320 MPa differential stress and temperatures ranging from 1373 to 1523 K. Creep data from experiment PI–612 are shown in Fig. 3b. An activation energy for dislocation creep was determined by fitting the log $\dot{\varepsilon}$ versus $1/T$ creep data using a least-squares algorithm.

Table 1 Creep data from all Ni_2GeO_4 experiments

Experiment no.	Jacket	$d_{initial}$ (μm)	d_{final} (μm)	Temp (K)	Stress (MPa)	Strain rate (s^{-1})	Corrected strain rate (s^{-1})	Total strain (%)
PI–604	Ni	7.4	7.4	1473	168	9.43×10^{-6}		
					55	2.75×10^{-6}		
					84	3.42×10^{-6}		
					112	4.21×10^{-6}		
					169	6.40×10^{-6}		
					199	8.72×10^{-6}		
					225	1.20×10^{-5}		
					286	1.77×10^{-5}		
					314	3.09×10^{-5}		18
					259	2.01×10^{-5}		
				1423	171	6.06×10^{-6}		
					85	1.98×10^{-6}		
					116	2.49×10^{-6}		
					174	4.22×10^{-6}		
					204	5.36×10^{-6}		
					233	7.21×10^{-6}		
					292	1.37×10^{-5}		
					326	1.88×10^{-5}		
PI–612	Ni	7.4	7.4	1523	224	6.07×10^{-5}		
				1473	225	1.55×10^{-5}		
					318	2.97×10^{-5}		
				1423	225	5.60×10^{-6}		
					319	8.49×10^{-6}		9.4
				1373	227	1.64×10^{-6}		
					320	2.33×10^{-6}		
				1398	229	3.16×10^{-6}		
					321	4.93×10^{-6}		
PI–621	Ni	5.6	5.8	1523	130	9.33×10^{-5}		
					61	3.87×10^{-5}		
				1473	132	2.22×10^{-5}		
					63	1.14×10^{-5}		
				1424	133	7.67×10^{-6}		
					63	3.15×10^{-6}		15
				1373	133	2.95×10^{-6}		
					62	1.18×10^{-6}		
				1422	132	1.25×10^{-5}		
					62	3.73×10^{-6}		
				1473	133	2.34×10^{-5}		
					62	9.92×10^{-6}		
PI–669	Cu	0.5	1.06	1123	141	1.40×10^{-5}	2.21×10^{-5}	
					45	3.46×10^{-6}	6.24×10^{-5}	
					68	6.09×10^{-6}	1.18×10^{-5}	
					114	9.51×10^{-6}	1.94×10^{-5}	
					172	1.35×10^{-5}	2.85×10^{-5}	
					230	1.27×10^{-5}	2.81×10^{-5}	
					289	1.40×10^{-5}	3.21×10^{-5}	
					174	8.28×10^{-6}	2.01×10^{-5}	
					93	4.77×10^{-6}	1.23×10^{-5}	18
				1173	175	2.18×10^{-5}	8.34×10^{-5}	
					46	5.44×10^{-6}	2.51×10^{-5}	
					70	6.90×10^{-6}	3.64×10^{-5}	
					117	9.10×10^{-6}	5.29×10^{-5}	
					237	1.19×10^{-5}	7.55×10^{-5}	
					166	8.33×10^{-6}	5.80×10^{-5}	
				1123	179	2.48×10^{-6}	1.86×10^{-5}	
					275	3.26×10^{-6}	2.48×10^{-5}	

Table 1 (Continued)

Experiment no.	Jacket	$d_{initial}$ (μm)	d_{final} (μm)	Temp (K)	Stress (MPa)	Strain rate (s^{-1})	Corrected strain rate (s^{-1})	Total strain (%)
PI–785	Ni	3.3	3.7	1274	161	1.54×10^{-6}	1.21×10^{-6}	
					210	1.56×10^{-6}	1.29×10^{-6}	
					255	1.70×10^{-6}	1.46×10^{-6}	
PI–785					156	8.14×10^{-7}	7.49×10^{-7}	7
					227	9.85×10^{-7}	9.49×10^{-7}	
					258	1.24×10^{-6}	1.24×10^{-6}	
PI–788	Cu	3.7	4.0	1274	175	1.10×10^{-6}	8.99×10^{-7}	
					216	1.04×10^{-6}	8.97×10^{-7}	
					269	1.08×10^{-6}	9.80×10^{-7}	6
					210	6.49×10^{-7}	6.23×10^{-7}	
					267	9.62×10^{-7}	9.62×10^{-7}	

Creep data were fit using a power-law equation of the form:

$$\dot{\varepsilon} = A\sigma^n \exp\left(-\frac{E^*}{RT}\right) , \quad (1)$$

where temperature (T), differential stress (σ), and strain rate ($\dot{\varepsilon}$) are independent variables. Oxygen fugacity was not included as an independent variable because it was held constant by the Ni/NiO buffer and was never varied. Values for the preexponential coefficient A, stress exponent n, and activation energy E^* are shown below.

$A = 10^{2.95\pm0.15}(\mathrm{MPa}^{-2.9}\,\mathrm{s}^{-1})$

$n = 2.9 \pm 0.1$

$E^* = 416 \pm 16$ (kJ mol^{-1}).

Experiments in the diffusion creep regime

Five experiments were conducted in the diffusional creep regime on samples with grain sizes ranging from 0.5 to 7.4 μm. One temperature-stepping test was performed at constant differential stress and four stress-stepping tests were performed at constant temperature. Since grain growth occurred in some of the fine-grained samples, similar temperature and stress conditions were revisited during the course of the experiment.

Correcting creep data for grain growth

In some fine-grained samples, sample hardening occurred during the experiment as a result of grain growth. Since we can only measure the grain size at the start and end of the experiment, it is necessary to calculate the grain size at each stress step by interpolating between the initial and final grain size. In such situations, the grain size was estimated as a function of time by assuming a grain-growth law of the following form:

$$d(t)^m - d_0^m = k_0 t , \quad (2)$$

where d_0 is the initial grain size, $d(t)$ is the grain size at time t, m is an exponent typically between 2 and 3, k_0 is a reaction constant, and t is time. The uncertainty in the exponent m contributes a very small error to the corrected creep rate (<5%) because creep rates are interpolated over a small range in grain size (a factor of 2). Creep data for a sample that had experienced grain growth were then corrected to a single grain size by using the formula:

$$\log \dot{\varepsilon}_{corr} = \log \dot{\varepsilon} - p \cdot \log\left(\frac{d(t)}{d_f}\right) , \quad (3)$$

where $\dot{\varepsilon}_{corr}$ is the corrected strain rate, $\dot{\varepsilon}$ is the uncorrected strain rate, p is the grain-size exponent for diffusion creep ($\dot{\varepsilon} \propto d^{-p}$), $d(t)$ is the grain size at the end of each stress step, and d_f is the grain size at the end of the experiment. When creep data are corrected to reflect a single grain size, the stress exponent can be determined through a least-squares linear regression. Corrected creep data were used only to constrain the stress exponent. The grain-size exponent and activation energy were obtained using creep data for which no correction was necessary.

Method for obtaining diffusion creep parameters

The large range in grain size and stress used for the diffusion creep experiments in this study made it impossible to have overlapping temperatures for every experiment. In particular, higher temperatures were necessary at larger grain sizes so that strain rates were measurable (e.g., above $\sim 1 \times 10^{-6}$ s^{-1}). It was therefore necessary to extrapolate creep data to a common temperature before the grain-size exponent could be determined.

Creep parameters were calculated according to the iterative procedure defined below. First, an average stress exponent was determined from log $\dot{\varepsilon}$ versus log σ data for several samples. An initial estimate of the activation energy for diffusion creep was then obtained over a limited temperature range using data from a temperature-stepping experiment. This activation energy was then used to estimate the grain-size exponent in the following way. First, strain rates corresponding to

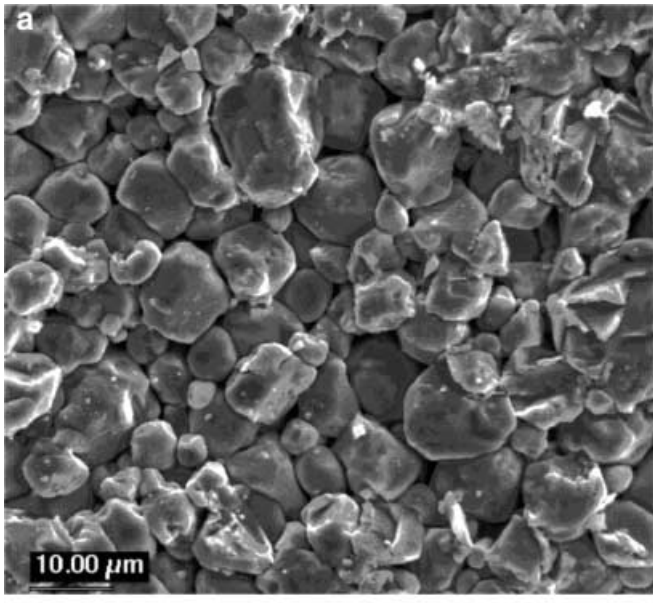

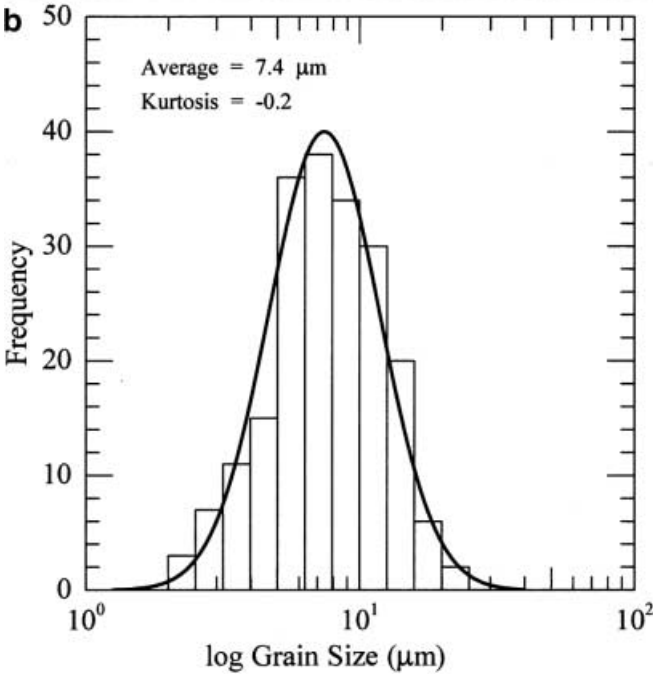

Fig. 2 **a** SEM micrograph of a fractured surface of sample PI–604 before deformation. Grains are typically equant and have a normal grain size distribution. **b** Grain-size distribution before deformation of sample PI–604. The distribution is log normal with a slight negative kurtosis. The reported average grain size corresponds to the logarithmic average

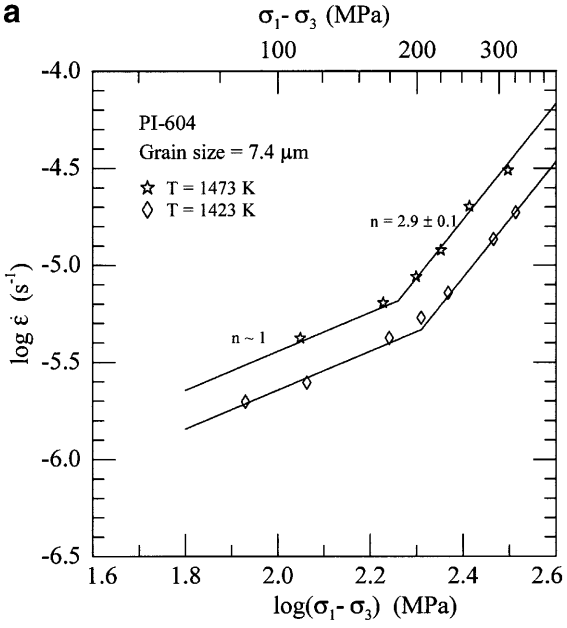

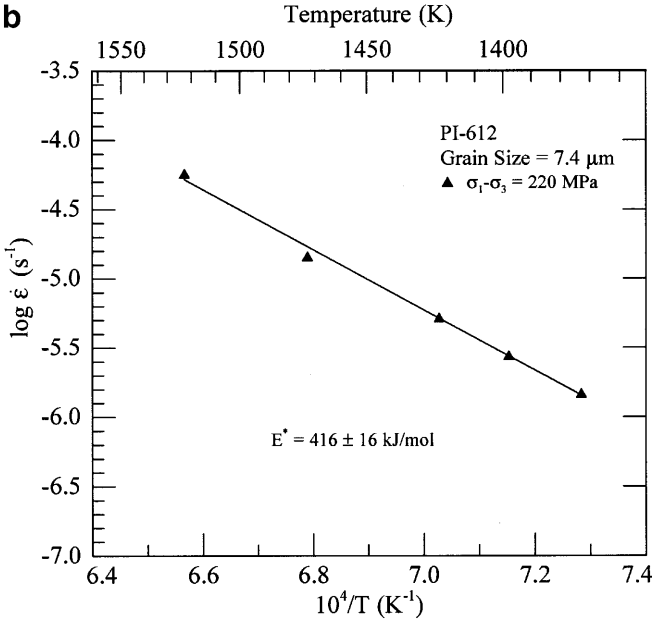

Fig. 3 **a** Plot of creep data from experiment PI–604, demonstrating a transition between diffusional creep ($n \sim 1$) at lower stresses and dislocation creep ($n = 2.9 \pm 0.1$) at higher stresses. **b** Creep data from experiment PI–612 are used to constrain the activation energy for dislocation creep

100 MPa differential stress were selected from each experiment. This value of differential stress was chosen because it was within the range of all mechanical data and involved no extrapolation. Strain rates were then extrapolated to $T = 1223$ K using our initial estimate for activation energy in the equation below:

$$\log \dot{\varepsilon}_{\text{norm}} = \log \dot{\varepsilon} - 0.43 \frac{E^*}{RT} \left(\frac{1}{1223} - \frac{1}{T} \right) , \qquad (4)$$

where E^* is the activation energy for diffusional creep. Normalized log creep rates are then plotted against $\log(d)$ for each sample. An initial estimate of the grain-size exponent p is obtained by fitting the data using a least-squares linear regression.

A new estimate for activation energy is obtained in a manner similar to that described above. First strain rates corresponding to 100 MPa differential stress are selected, then extrapolated to a grain size of 2 μm using the following equation:

$$\log \dot{\varepsilon}_{\text{norm}} = \log \dot{\varepsilon} - p[\log(2) - \log(d)] \ , \qquad (5)$$

where p is the grain-size exponent determined in the previous step and d is the grain size for each experiment. We chose a grain size of 2 μm so that the amount of extrapolation was minimized. We plot log $\dot{\varepsilon}_{\text{norm}}$ versus $1/T$ to obtain a new estimate for the activation energy for diffusional creep. Equations (4) and (5) are iterated until a convergent solution is found. To test this method, we used an initial estimate for the grain-size exponent instead of the activation energy. When $p = 2$ was used as a starting value, the solution converged to the same result as in the former case.

Results for diffusion creep

The stress exponent was first estimated from experiments in which minimal grain growth was observed. These experiments, which represent the majority of the dataset, indicate a stress exponent $n \sim 1$. We subsequently refined our estimate of the stress exponent by including corrected creep data from samples that had experienced grain growth during the course of the experiment. Mechanical data from samples that were deformed in the diffusional creep regime are plotted in Fig. 4a. Creep data were fit using a least-squares linear regression, yielding slopes between $n = 0.7$ and $n = 1.2$, with an average $n = 1.0 \pm 0.2$.

We obtained an activation energy for diffusion creep using the iterative procedure described in the previous section. Normalized creep rates are plotted in Fig. 4b, from which an activation energy $E^* = 281 \pm 11\,\text{kJ mol}^{-1}$ was determined using a least-squares linear regression, excluding data at 1523 K. We report an activation energy only for temperatures between 1123 and 1473 K because there is some evidence for a change in activation energy at temperatures above 1473 K.

The grain-size exponent was also determined using an iterative procedure. Normalized creep data are plotted in Fig. 4c, from which a grain-size exponent $p = 3.0 \pm 0.2$ was determined by least-squares linear regression. When creep data from samples that have experienced grain growth are analyzed, a grain-size exponent can be determined based on the initial and final grain size. This analysis, which assumes that all

►

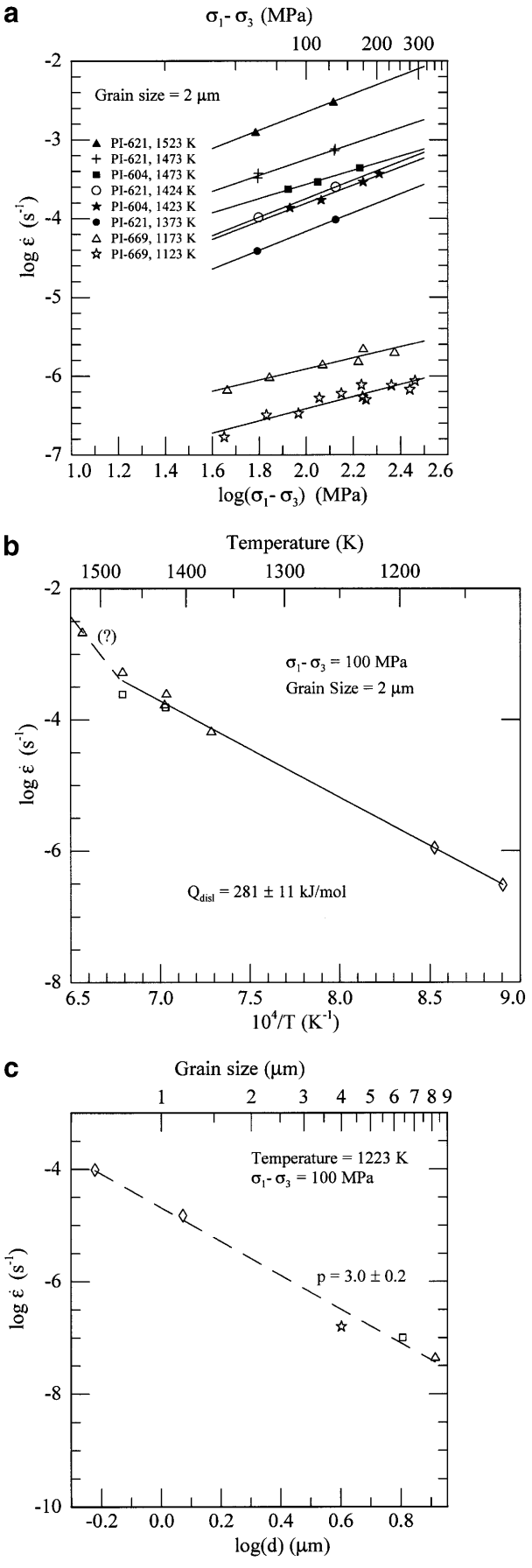

Fig. 4 **a** Diffusion creep data from all experiments are shown to illustrate the typical variation in stress exponent. Slopes determined from a least-squares regression vary from $n = 0.7$ to 1.2, with an average of $n = 1.0 \pm 0.2$. Creep data were normalized to a grain size of 2 μm so that all data could be shown on one plot. **b** The activation energy for diffusion creep was determined using creep data from three experiments, extrapolated to a single stress and grain size (*triangles* are from PI–621, *squares* from PI–604, *diamonds* from PI–669). The *dashed line* represents a possible change in activation energy above 1473 K. **c** The grain-size exponent for diffusion creep was determined using creep data from four experiments, extrapolated to a single temperature and stress (*diamonds* are from PI–669, *square* from PI–621, *triangle* from PI–604, *star* from PI–785). A grain-size exponent $p = 3.0 \pm 0.2$ suggests that deformation occurred by Coble creep

sample hardening is due to grain growth, is fully consistent with a grain-size exponent $p = 3$.

We used copper jackets for deformation experiments on some fine-grained samples because the samples had strengths that were comparable to the nickel jackets. Since copper jackets buffer the oxygen fugacity at higher values, we needed to test if there was an effect of oxygen fugacity on diffusion creep. Two deformation experiments were performed using different oxygen buffers. The same sample was used in both experiments to minimize discrepancies due to sample-to-sample variation. In the first experiment, an Ni jacket was used so that the oxygen fugacity was fixed by the Ni/NiO buffer. We chose a deformation temperature $T = 1273$ K because it was lower than the melting point of copper but high enough so that strain rates were measurable. Because the grain size increased slightly during the experiment, creep data were corrected to a grain size of 4 μm. The sample was then rejacketed in copper so that the oxygen fugacity was fixed by the Cu/Cu_2O buffer. The sample was held at temperature for more than 2 h so that the internal point defects could equilibrate to the new oxygen fugacity. Creep data were corrected to a grain size of 4 μm as in the previous case.

Creep data for both experiments are shown in Fig. 5. They are virtually indistinguishable, indicating that there is no measurable oxygen fugacity dependence in the diffusion creep regime. No correction was therefore necessary for samples surrounded by different metal jackets.

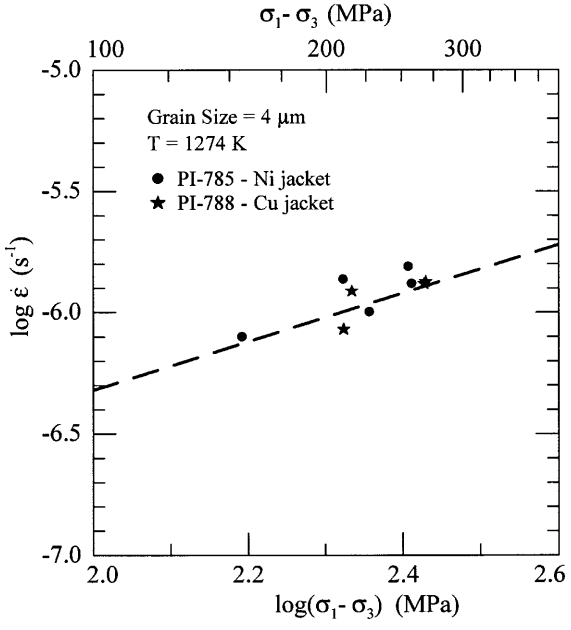

Fig. 5 The use of copper or nickel jackets has no noticeable effect on the creep rate, indicating that there is little to no dependence of oxygen fugacity on creep rate for nickel germanate. Creep data were corrected to a grain size of 4 μm using a grain-size exponent $p = 3$

Creep data were fit by a diffusion creep equation of the following form, which assumes a linear stress dependence:

$$\dot{\varepsilon} = A\frac{\sigma^n}{d^p} f_{O_2}^m \exp\left(-\frac{E^*}{RT}\right) \quad , \tag{6}$$

where temperature (T), differential stress (σ), strain rate ($\dot{\varepsilon}$), oxygen fugacity (f_{O_2}), and grain size (d) are independent variables. Values for diffusion creep parameters are shown below:

$$A = 10^{5.53\pm0.21}\left(\frac{\mu m^3}{MPa\ s^{-1}}\right)$$

$$n = 1.0 \pm 0.2$$

$$p = 3.0 \pm 0.2$$

$$m \cong 0$$

$$E^* = 281 \pm 11 (kJ\ mol^{-1}).$$

Discussion

Deformation at high temperatures can occur either by the progressive movement of dislocations in response to an applied stress (dislocation creep), or by the movement of point defects along grain boundaries or through the lattice (diffusion creep). The former process is characterized by a power-law dependence of stress on strain rate, while the latter process features a linear dependence of stress on strain rate. In samples with certain grain sizes, it is possible to observe dislocation creep at higher stress and diffusion creep at lower stress. By performing a stress-stepping test at a fixed temperature, one can estimate the transition stress between the two deformation mechanisms.

Initially, we chose a relatively coarse-grained sample with an average grain size of 7.4 μm. Stress-stepping tests revealed a change in slope from $n \sim 1$ to $n \sim 3$ at a stress near 200 MPa, indicating a change in mechanism from diffusion creep to dislocation creep. The stress exponent ($n = 2.9 \pm 0.2$) obtained from the high-stress creep data is similar to values predicted from standard theoretical models ($3 < n < 5$) (Nabarro 1967; Weertman 1968).

Reliable estimates of the activation energy are necessary because flow laws are often extrapolated to lower temperatures, particularly when modeling the dynamics of slab deformation. At the temperatures of our experiments ($T/T_m = 0.75$), a 100-K increase in temperature results in an order of magnitude increase in strain rate. The effect of temperature on strain rate would, of course, be magnified at lower temperatures due to its exponential dependence.

At low stress and small grain size, nickel germanate exhibited a linear stress-strain dependence with a stress

exponent $n = 1.0 \pm 0.2$, which is characteristic of diffusion creep. In the diffusion creep regime, deformation is sensitive to grain size, so that any increase in grain size due to grain growth results in a lowering of the creep rate.

There are two possible mechanisms for diffusion creep. Mass can be transported by the motion of point defects through the lattice (Nabarro-Herring creep) or along grain boundaries (Coble creep). Nabarro-Herring and Coble creep are characterized by a grain-size-dependent creep rate, in which the grain-size exponent $p = 2$ and 3, respectively, for each process. We determined a grain-size exponent of 3 for nickel germanate spinel, suggesting that deformation occurs by a Coble creep mechanism. A grain-size exponent $p = 3$ is also consistent with grain-boundary sliding accommodated by volume and grain-boundary diffusion (Ashby and Verrall 1973). The Ashby and Verrall model has several shortcomings, however, and does not fit existing experimental data very well (Gifkins 1978). Grain-boundary sliding also tends to operate in systems that have equant grain shape and that do not exhibit normal grain growth. While we cannot eliminate the possibility of diffusion-accommodated grain-boundary sliding as the predominant deformation mechanism, it is more likely that diffusion creep mechanisms occur in our samples. This hypothesis could be tested if grain-boundary diffusion rates in nickel germanate were known.

We determined an activation energy for diffusion creep of 281 kJ mol^{-1}. There is some evidence for a change in activation energy above 1473 K, but since this is based on a single data point, we prefer to report an activation energy based on temperatures between 1123 and 1473 K only. Further experiments at temperatures above 1473 K are necessary to determine if there is change in activation energy.

Effect of oxygen fugacity on diffusion creep

In certain materials, oxygen fugacity can have a profound effect on the creep rate. This effect was shown for transition-metal-bearing olivines (Ricoult and Kohlstedt 1985), demonstrating the need for establishing thermodynamic equilibrium during creep experiments. In such experiments, the silica activity usually is controlled by the presence of a few volume percent pyroxene grains. Ideally, the activity of germania should also be fixed in a similar manner by adding a few percent pyroxene grains. No pyroxene phase exists at low pressures in the NiO–GeO_2 system; hence, the activity of germania could be fixed at unity only if excess GeO_2 were present in the sample. It is difficult to incorporate excess GeO_2 for two reasons, however. Because of the extensive evaporation of germania during the synthesis stage, no excess GeO_2 remains. In addition, if excess GeO_2 powder were added to the nickel germanate powder before hot-pressing, the low melting temperature of GeO_2 would cause extensive melting under most deformation conditions. Although the activity of germania remains unbuffered, the presence of NiO powder surrounding the sample ensures that the activity of NiO remained constant.

We chose two metal-oxide buffers, Ni/NiO and Cu/Cu_2O, so that we could equilibrate our sample at two different oxygen fugacities (for a discussion of equilibration kinetics using solid buffers, see Karato et al. 1986). At 1 atm pressure and 1273 K, the oxygen fugacity corresponding to the Cu/Cu_2O buffer is 3.2 log units higher than that of the Ni/NiO buffer. At 300 MPa pressure, the oxygen fugacities for metal-oxide systems do not change substantially from their room temperature values, so we approximate the difference as 3.2 log units. From Fig. 5, we observe that there is little difference in the creep rate between a copper-or nickel-jacketed sample. This indicates that there is little to no oxygen fugacity dependence in Ni–Ge spinel. Electroneutrality conditions involving Frenkel defects, or $[Ni''_{Ge}]$ paired with $[V^{\cdot\cdot}_{O}]$, $[Ni^{\cdot\cdot}_{i}]$ or $[Ge^{\cdot\cdot\cdot\cdot}_{i}]$ produce a zero oxygen fugacity dependence. For a similar example in a different spinel system, see Greskovich and Schmalzried (1970). Although we cannot rule out a 1/10 dependence due to experimental scatter, we can rule out a 1/6 dependence because this would result in a change in strain rate of 0.53 log units, well above the resolution capability of the Paterson apparatus. The absence of an oxygen fugacity dependence on creep rate in Ni germanate spinel is consistent with the results of Wolfenstine and Kohlstedt (1994) for Ni silicate olivine.

Comparison with other spinels

Previous microstructural investigations of several spinels reveal dislocation microstructures consistent with a $[1\ 1\ 0]\langle 1\ 1\ 1\rangle$ slip system (Hwang et al. 1975; Vaughan and Coe 1981; Karato et al. 1998). In addition, the dissociation of straight-edge dislocations into two colinear partials is seen in a number of spinels (Veyssière et al. 1978; Doukhan et al. 1979; Dupas-Bruzek et al. 1998). These observations have provided a basis for the use of spinel analogues by previous researchers (Vaughan and Coe 1981; Dupas-Bruzek et al. 1998). There has, however, been no examination of the normalized creep behavior of spinel, particularly in the germanate system, which is often used as an analogue for silicate spinel. By normalizing the shear stress and temperature by the shear modulus and melting temperature, respectively, materials with similar structures often have similar normalized creep strengths (they are isomechanical). We therefore compare the mechanical data for nickel germanate and several normal and inverse spinels to see if an isomechanical group can be defined.

Dislocation creep data have been collected for several spinels at temperatures $T/T_m \sim 0.5$–0.9 (Mitchell et al. 1976; Nishikawa et al. 1980; Dupas-Bruzek et al. 1998). Although the temperature range for each data set is typically limited to ~100 K, three of the four datasets

have homologous temperatures that overlap. Since the mechanism of dislocation creep is the same for these spinels, it is reasonable to compare their creep parameters as well as their absolute strength.

Stress exponents are similar for $Mn_{0.5}Zn_{0.5}Fe_2O_4$, Ni_2GeO_4 and Mg_2GeO_4 spinels ($n \sim 3$) and slightly higher for $MgAl_2O_4$ ($n \sim 4$). Stress exponents in the range $3 < n < 5$ are indicative of recovery-controlled creep, where steady-state deformation results from a balance between dislocation multiplication and climb-controlled recovery processes. Although small differences in the stress exponent are relatively unimportant at experimental strain rates, the difference can become significant when extrapolating to natural strain rates. For example, $MgAl_2O_4$ is 100 times stronger than Ni_2GeO_4 at $\dot{\varepsilon} = 10^{-15}$ s^{-1}, while it has a comparable strength at $\dot{\varepsilon} = 10^{-5}$ s^{-1}.

Activation energies for dislocation creep can be compared by normalizing them by RT_m, yielding the nondimensional parameter g:

$$g = \frac{Q_{\text{distl}}}{RT_m} \quad .$$

Values for g are similar for Ni_2GeO_4 ($g \sim 26$) and $Mn_{0.5}Zn_{0.5}Fe_2O_4$ ($g \sim 24$), but different from $MgAl_2O_4$ ($g \sim 42$). The large value of g for $MgAl_2O_4$ may reflect a fundamental difference between $MgAl_2O_4$ and other spinels, or it may result from a change in the rate-limiting creep mechanism at high temperatures ($T/T_m \sim 0.85$–0.90). Creep experiments on $MgAl_2O_4$ at lower temperatures ($T/T_m \sim 0.7$–0.8) are needed for a valid comparison of activation energy. Since temperatures in subducting slabs ($T/T_m \sim 0.4$–0.7) are typically lower than experimental temperatures ($T/T_m \sim 0.7$–0.9), it is desirable to measure activation energies at the lowest possible temperatures to minimize extrapolation errors. Since all available g values are in the range of 24 to 26 at $T/T_m \sim 0.7$–0.8, they represent the best current estimates for g for silicate spinel.

To define an isomechanical group it is necessary to compare the strength of several materials with similar structures. We chose creep data for $MgAl_2O_4$, $Mn_{0.5}Zn_{0.5}Fe_2O_4$, Mg_2GeO_4, and Ni_2GeO_4 spinel, extrapolated to a strain rate $\dot{\varepsilon} = 10^{-5}$ s^{-1}. There is a general agreement between the normalized creep strengths of all four spinels, shown in Fig. 6a. Two of the normal spinels (Ni_2GeO_4 and $MgAl_2O_4$) show higher creep strengths than the inverse spinels ($Mn_{0.5}Zn_{0.5}Fe_2O_4$), although the difference is relatively minor (less than 1 order of magnitude). Magnesium germanate, which is normal type, has a lower stress, consistent with inverse ferrite spinel. The authors acknowledged, however, that glassy phases were present along grain boundaries, which may have contributed to a lower creep strength (Dupas-Bruzek et al. 1998). Thus, it is not possible to evaluate whether there is a systematic difference in strength between normal and inverse spinels or simply a difference between ferrite and other spinels. Creep tests on inverse spinels with a point-defect chemistry that is

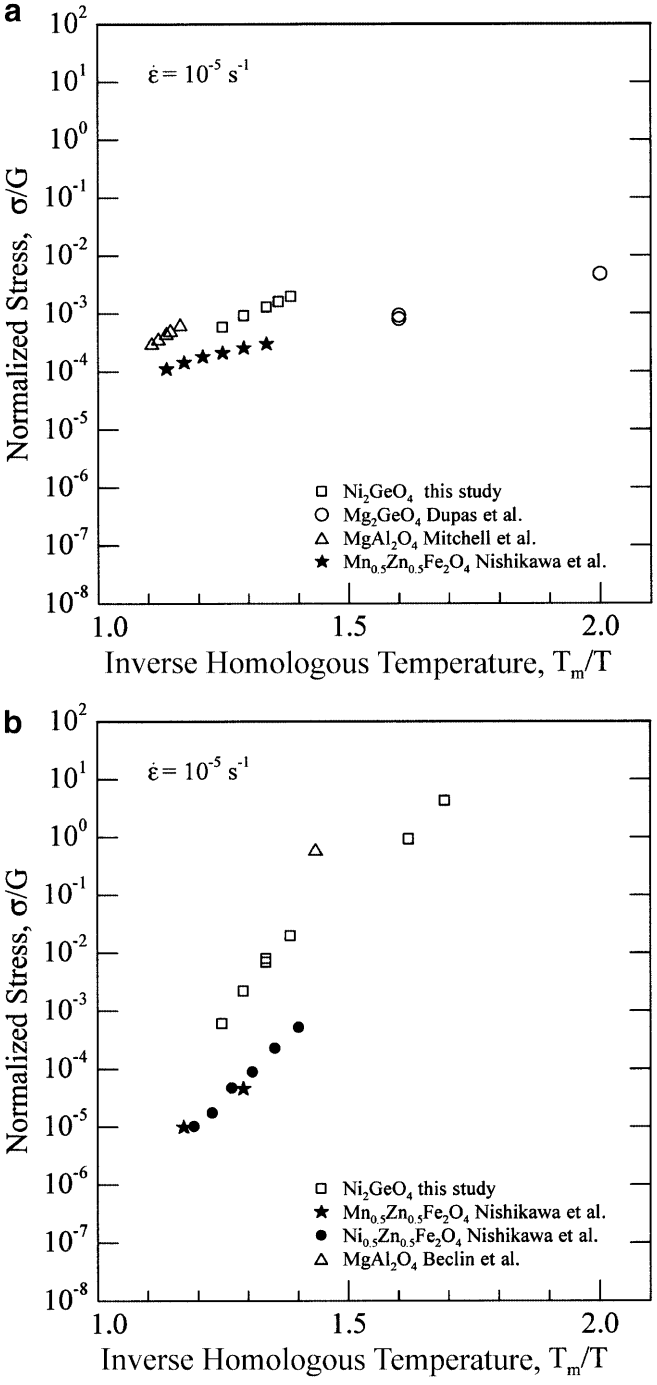

Fig. 6 **a** Normalized dislocation creep data for Ni_2GeO_4, Mg_2GeO_4, $MgAl_2O_4$, and $Mn_{0.5}Zn_{0.5}Fe_2O_4$ spinels. Creep data were extrapolated to a strain rate of 10^{-5} s^{-1} using stress exponents listed in Table 2. Stress and temperature were normalized by the shear modulus and melting temperature of each material. An isomechanical group can be defined for spinels, characterized by a 1 order-of-magnitude variation in normalized strength. **b** Normalized diffusion creep data for Ni_2GeO_4, $MgAl_2O_4$, $Ni_{0.5}Zn_{0.5}Fe_2O_4$ and $Mn_{0.5}Zn_{0.5}Fe_2O_4$ spinels. Creep data were extrapolated to a common strain rate and d/**b** ratio, where d is grain size and **b** is the Burger's vector. Creep data for Ni_2GeO_4 were extrapolated to a grain size of 10 μm. Stress and temperature were normalized by shear modulus and melting temperature of each material. Normal and inverse spinels are indicated by *open* and *closed symbols*, respectively

similar to normal spinels must be performed (ferrites are *n* type while the normal spinels presented here are not).

Duclos et al. (1978), Duclos (1981), and Okamoto (1989) provide evidence that dislocation creep in spinel might be due to dislocation climb (as opposed to glide) proposed by Nabarro (1967). Cannon and Langdon (1988) argue that creep in ceramics showing $n \sim 3$ may be due to dislocation climb from Bardeen-Herring sources, as proposed by Nabarro (1967). To test this hypothesis, we calculated the effective diffusion coefficients from dislocation creep data using the theoretical relationship by Nabarro (1967):

$$\dot{\varepsilon} = \frac{BV_m D_{eff}\sigma^3}{G^2\mathbf{b}^2 RT} \quad ,$$

where $B \sim 0.3$, V_m, is the molar volume, D_{eff} is the effective diffusion coefficient, σ is stress, G is the shear modulus, **b** is the Burger's vector and R is the gas constant. The results are shown in Fig. 7. The results agree well with the oxygen self-diffusion coefficients in $MgAl_2O_4$ spinel after normalization, supporting the notion that dislocation creep in nickel germanate spinel may be due to dislocation climb.

An important consequence of the dislocation climb model of dislocation creep in spinel is that the deformation fabric is pure shear and is associated with no vorticity. This point will have to be tested by fabric measurements. The results will have an important implication for seismic anistropy in the transition zone.

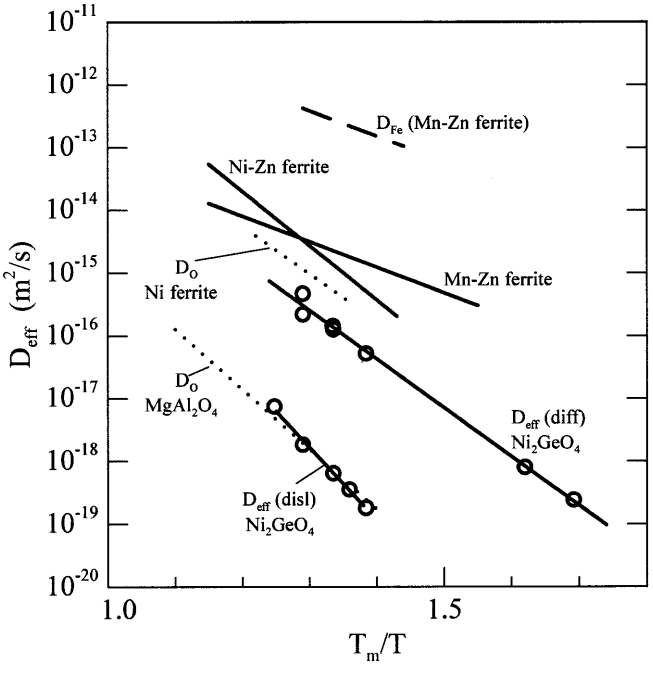

Fig. 7 Effective diffusion coefficients calculated from diffusion creep data using Nabarro's model (1967): Mn–Zn ferrite [$E^* = 217$ KJ mol^{-1}] (Nishikawa et al. 1980); Ni–Zn ferrite [$E^* = 36$ kJ mol^{-1}] (Nishikawa et al. 1979); Ni_2GeO_4 [$E^* = 281$ kJ mol^{-1}] (this study). Effective diffusion coefficient calculated from dislocation creep data using a Nabarro dislocation climb model (1967): Ni_2GeO_4 [$E^* = 416$ kJ mol^{-1}] (this study). Lattice self-diffusion coefficients for oxygen and iron in $MgAl_2O_4$ and Mn–Zn ferrite are shown for reference: D_O in $MgAl_2O_4$ [$E^* = 439$ kJ mol^{-1}] (Ando and Oishi 1983); D_O in Ni ferrite [$E^* = 255$ kJ mol^{-1}] (O'Bryan and Dimarcello 1970); D_{Fe} in Mn–Zn ferrite: [$E^* = 147$ kJ mol^{-1}] (Ogawa et al. 1968)

Diffusion creep parameters for several spinels are shown in Table 3. A stress exponent $n \sim 1$ and a grain-size exponent $p \sim 3$ indicate that deformation occurs by Coble creep, rather than Nabarro-Herring creep (where $p \sim 2$). Although diffusion creep parameters are generally similar for all spinels, normalized creep strengths show greater variation. Diffusion creep data for four spinels were extrapolated to a strain rate of $\dot{\varepsilon} = 10^{-5}$ s^{-1} and a $d/\mathbf{b}$ ratio of 1.72×10^{-4}, where d is grain size and **b** is the Burger's vector. This ratio corresponds to a grain size close to 10 μm. There is a general agreement in mechanical strength among the four spinels, as indicated in Fig. 6b, but the scatter is somewhat larger than for the case of dislocation creep (roughly 2 orders of magnitude in flow stress). Ferrite spinels have a similar strength, while Ni_2GeO_4 and $MgAl_2O_4$ spinel are stronger by two orders of magnitude. Both ferrites are inverse spinels, and they also have similar point-defect chemistry. Since Fe^{3+} has a strong tetrahedral site preference, it is forced to occupy both tetrahedral and octahedral sites (Navrotsky 1967). The Fe^{3+} on the octahedral site can achieve a lower energy state by acting as an electron acceptor, thus behaving like an *n*-type material. Therefore, creep rates for ferrites may vary substantially with oxygen fugacity if electrons are one of the majority point defects. This difference in point-defect chemistry between the ferrites and Ni_2GeO_4 may explain the discrepancy in normalized creep behavior.

The difference in normalized creep strength may also be related to such factors as oxygen fugacity, grain boundary width, or nonstoichiometry (Doukhan et al. 1976; Chiang and Kingery 1990). In manganese ferrite, for instance, oxygen grain-boundary diffusion is significantly reduced by the addition of less than 1 wt% SiO_2 or $CaCO_3$ (Boy and Wirtz 1994). This illustrates the important role of sample preparation in obtaining reliable and consistent results in the diffusion creep regime. It is also possible that a better correlation may be obtained by comparing other II–IV spinels with nickel germanate, particularly those that have a zero oxygen fugacity dependence. Creep experiments on Fe_2GeO_4 spinel are planned to test this hypothesis.

When diffusion creep is accommodated by diffusive mass transfer, standard theoretical models predict a flow law of the following form (see, e.g., Karato et al. 1986):

$$\dot{\varepsilon} = A\frac{V_m D_{eff}\sigma}{RTd^2} \quad ,$$

where A is a numerical constant dependent on the flow geometry (at small strain, $A = 14$ for diffusion creep: Raj and Ashby 1971), V_m is molar volume, D_{eff} is an effective diffusion coefficient composed of a volume diffusion and a grain-boundary diffusion term, σ is stress, d is grain size and RT has the usual meaning. When D_{eff} is dominated by a grain-boundary diffusion

Table 2 Dislocation creep parameters for several spinels

Spinel	T_m (K)	G (GPa)	n	$Q \sim g \cdot RT_m$	Reference
Ni_2GeO_4	~1900	~100	2.9 ± 0.2	$26 \cdot RT_m$	This study
Mg_2GeO_4	~2400	110	~3	–	Dupas-Bruzek et al. (1998)
$Mn_{0.5}Zn_{0.5}Fe_2O_4$	~1900	64	2.6 ± 0.2	$24 \cdot RT_m$	Nishikawa et al. (1980)
$MgAl_2O_4$	~2400	108	3.9	$42 \cdot RT_m$	Mitchell et al. (1976)

Table 3 Diffusion creep parameters for several spinels

Spinel	T_m (K)	$Q \sim g \cdot RT_m$	n	p	Reference
Ni_2GeO_4	~1900	$18 \cdot RT_m$	1.0 ± 0.2	3.0 ± 0.2	This study
$Ni_{0.5}Zn_{0.5}Fe_2O_4$	~1990	$19 \cdot RT_m$	1.1 ± 0.1	~3	Nishikawa et al. (1979)
$Mn_{0.5}Zn_{0.5}Fe_2O_4$	~1900	$14 \cdot RT_m$	1.1 ± 0.1	~3	Nishikawa et al. (1980)
$MgAl_2O_4$	~2400	?	~1	~3	Mitchell et al. (1976)

term, $D_{\text{eff}} \propto \delta D_{\mathbf{b}}/d$, where δ is a grain-boundary width and $D_{\mathbf{b}}$ is a grain-boundary diffusion coefficient. Therefore, $\dot{\varepsilon} \propto d^{-3}$ when diffusion is rate-limited by grain boundary diffusion and $\dot{\varepsilon} \propto d^{-2}$ when diffusion is rate-limited by volume diffusion.

Effective diffusion coefficients were calculated for three spinels as a function of homologous temperature, shown in Fig. 7. Both ferrites have a higher effective diffusion coefficient than nickel germanate, which is consistent with their weaker creep strength. Self-diffusion coefficients for lattice diffusion of oxygen and iron are shown in Fig. 7 for comparison. Effective diffusion rates calculated from ferrite creep data are intermediate between iron self-diffusion (D_{Fe}) and oxygen self-diffusion (D_{o}) in ferrite spinel. Since lattice diffusion of the cation species is faster than the effective diffusion rate, it is likely that grain boundary diffusion of oxygen is rate-limiting for ferrites. Similarly, grain-boundary diffusion of oxygen is rate-limiting for $MgAl_2O_4$, although overall creep rates and diffusion rates are slower. Since there are no available data for lattice or grain-boundary diffusion of oxygen in germanates, we can only speculate that diffusion rates are intermediate between that of $MgAl_2O_4$ and ferrite spinel (the creep rate is also intermediate between the two). Although it is impossible to rule out Ge as a rate-limiting species, it is likely that the cation species will be transported through the lattice, as it is in ferrite spinels. Tracer diffusion experiments are needed for II–IV spinels to test whether oxygen is the slowest diffusing species, as it is in II–III spinels.

Comparison of olivine and spinel strength

A preliminary assessment of the narmalized creep strengths of olivine and spinel was made by Karato (1989). This study was based on an extensive datset for olivines that contained different cations and a somewhat limited dataset for spinels, characterized primarily by II–III spinels. Since this time, more datasets have become available for spinel, including that of the present study. In light of those new data, we shall reexamine the normalized creep behavior of olivine and spinel in the dislocation and diffusion creep regimes, and extrapolate each isomechanical group to conditions that are appropriate for the Earth.

Dislocation creep flow laws for Co_2SiO_4 (Ricoult and Kohlstedt 1985) and $(Mg_{0.9}Fe_{0.1})_2SiO_4$ dunite (Chopra and Paterson 1984) were used to construct an isomechanical group for olivine. These two flow laws were chosen because they represent the strongest and weakest creep data (after normalization) from a range of synthetic and natural olivines. For a compilation of the normalized strength of olivine with several different compositions, the reader may refer to Bai and Green (1998). Creep data for synthetic olivine with an upper mantle composition (e.g., Karato et al. 1986) fall within these upper and lower bounds and are not represented in Fig. 8a for the sake of clarity. When the two flow laws are extrapolated to a strain rate $\dot{\varepsilon} = 10^{-15}\,\text{s}^{-1}$, the discrepancy between them becomes greater because of the difference in stress exponents ($n = 3.6$ for dunite and $n = 5$ for Co_2SiO_4). However, the true normalized strength for olivine is likely to be bracketed by these two flow laws.

Dislocation creep flow laws for Ni_2GeO_4 (this study) and $MgAl_2O_4$ (Mitchell et al. 1976) were used to construct an isomechanical group for spinel. These spinels were chosen because they have a normal structure, which is more applicable to the Earth. Flow laws for spinel also deviate from each other when they are extrapolated to Earth-like strain rates, because of their different stress exponents. Isomechanical groups for olivine and spinel, shown in Fig. 8a, were calculated between $T/T_m = 0.4$ and $T/T_m = 0.7$. Although there is a range in strength for each isomechanical group when flow laws are extrapolated to Earth-like strain rates, the olivine and spinel fields overlap, indicating that they

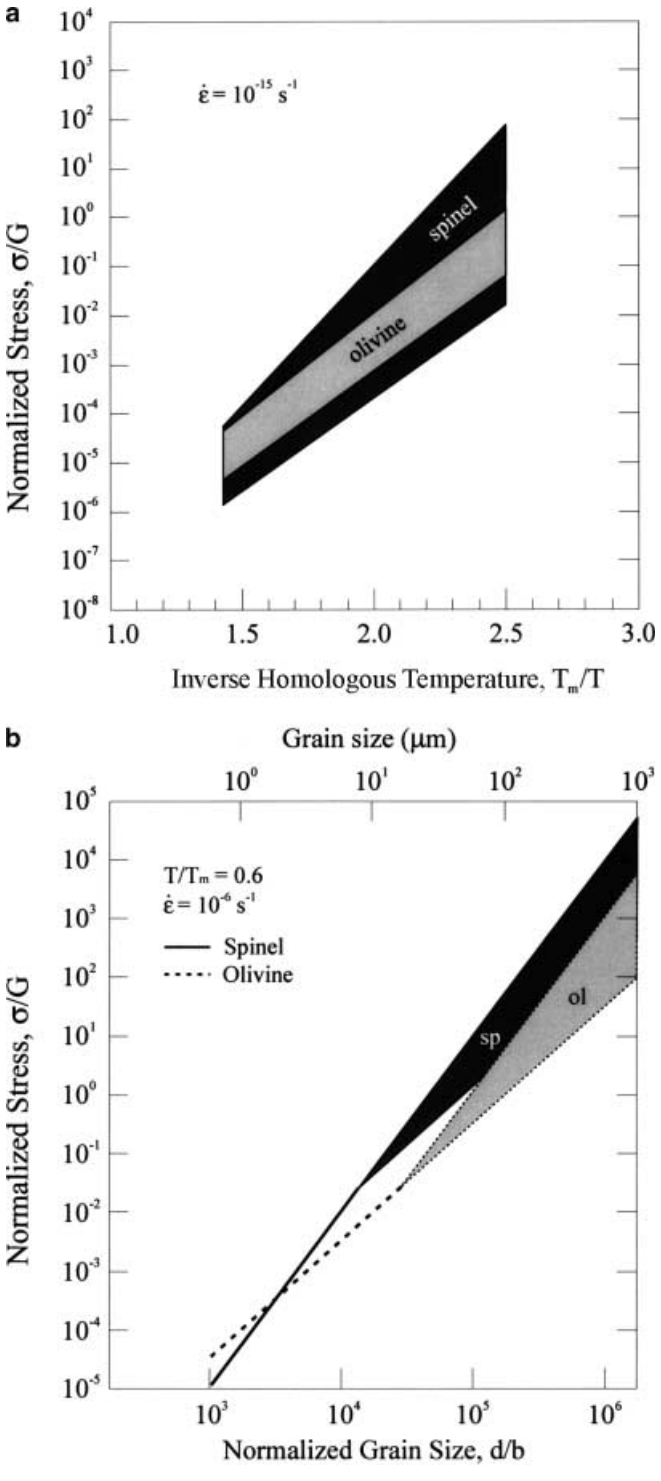

Fig. 8 **a** Comparison of normalized creep strengths for olivine and spinel in the dislocation creep regime, extrapolated to a strain rate of 10^{-15} s^{-1}. The spinel field is bracketed by flow laws for $MgAl_2O_4$ (Mitchell et al. 1976) and Ni_2GeO_4 (this study) while the olivine field is bracketed by flow laws for $(Mg, Fe)_2SiO_4$ (Chopra and Paterson 1984) and Co_2SiO_4 (Ricoult and Kohlstedt 1985). The olivine and spinel fields overlap each other, indicating that their normalized creep strength is comparable. Because spinel has a higher shear modulus, its actual flow stress is higher than olivine (by a factor of 1.5). **b** Comparison of normalized creep strengths for Mg_2GeO_4 olivine and Ni_2GeO_4 spinel in the diffusion creep regime. The *thicker lines* represent best fits through the experimental data, while the *dashed lines* represent extrapolations to larger grain sizes using grain-size exponents $p = 2$ and $p = 3$. Olivine and spinel have a comparable strength at 2 μm (unextrapolated creep rates are similar). Because of its smaller grain size exponent ($p = 2$ for olivine and $p = 3$ for spinel), olivine may be considerably weaker than spinel (up to 2.5 orders of magnitude) at grain size of 1 mm. At a strain rate of 10^{-15} s^{-1}, flow stresses would be 9 orders of magnitude smaller than that shown in the figure

have comparable normalized strengths. Since spinel has a shear modulus that is 50% greater than olivine, its unnormalized strength is actually greater than that of olivine.

Although olivine and spinel have comparable strengths in the dislocation creep regime, they do not always have comparable strengths in the diffusion creep regime. Normalized creep data for Mg_2GeO_4 olivine (Kizhappali and Karato 1996) and Ni_2GeO_4 spinel (this study) were compared as a function of grain size at $T/T_m = 0.6$. Unextrapolated creep data for olivine and spinel are shown by the solid and alternating dash and dotted lines in Fig. 8b. At a grain size of 2 μm, olivine and spinel have a comparable strength. Spinel is considerably stronger than olivine at coarse grain sizes (1 mm) because it deforms by Coble creep ($p = 3$) instead of Nabarro–Herring creep ($p = 2$), as is the case for olivine. Since a change in diffusion creep mechanism is possible for either olivine or spinel, creep data are extrapolated using grain-size exponents of $p = 2$ and $p = 3$ to bracket their strength. The strength of spinel (indicated by the dark gray region in Fig. 8b) is greater than that of olivine (shown in light gray) at coarse grain size. If flow laws are extrapolated to 1-mm grain size with no change in the grain-size exponent for either olivine or spinel, spinel will have a normalized strength that is 2.5 orders of magnitude stronger than olivine. Conversely, if grain-size reduction occurs, spinel can become weaker than olivine. This phenomenon may have important consequences for subducting slabs that are undergoing simultaneous deformation and transformation from olivine to spinel (e.g., Karato et al. 2000).

Conclusions

We have performed deformation tests on nickel germanate. A wide range of experimental conditions (temperature, stress, and grain size) were employed in order to characterize the dislocation creep and diffusion creep regimes. Five main conclusions can be drawn from this work:

1. High-resolution tests can be performed on nickel germanate spinels using a gas-medium deformation apparatus. At lower confining pressure, creep parameters for spinel can be determined more precisely.

2. The transition between diffusion creep and dislocation creep was identified for nickel germanate. For a sample with a grain size of 7.4 μm, the transition occurs at $\sigma = 200$ MPa at 1423 K and $\sigma = 180$ MPa at 1473 K.
3. Two experiments were performed to determine the oxygen fugacity dependence on creep rate in nickel germanate spinel. These experiments suggest that there is no oxygen fugacity dependence on creep rate in the diffusion creep regime.
4. An isomechanical group can be defined for spinels when creep data are normalized by the melting temperature and shear modulus. There is evidence for a difference between the normalized strength of normal and inverse spinels, in that normal spinels are slightly stronger.
5. Normalized creep strengths for olivine and spinel are comparable in the dislocation creep regime. In the diffusion creep regime, spinel is stronger than olivine at coarse grain sizes, but weaker than olivine at grain sizes below 2 μm.

Germanates are good analogues for the deformation behavior of silicate spinel because they have similar slip systems and because they form an isomechanical group with other spinels. Since silicate spinel is likely to belong to this isomechanical group, we can predict its strength by using normalized creep parameters obtained from analogue spinels. Nickel germanate spinel is a useful analogue from the standpoint of its low-pressure stability, but suffers from the fact that no pyroxene phase is stable at low pressures. Consequently, GeO_2 excess compositions will tend to melt due to the low melting temperature of GeO_2. Even at temperatures lower than the melting temperature, the high vapor pressure of GeO_2 may encourage vapor-phase transport, a condition that may not occur in silicate systems. By using an appropriate Mg–Ni or Mg–Fe solid solution, however, it is possible to form a stable pyroxene phase. Such a material would be an ideal analogue because it would be possible to deform a pyroxene-bearing aggregate at low pressures. In addition, compositions that are closer to Earth spinels can be selected, thereby providing a better estimate of the strength of spinel under Earth-like conditions.

Acknowledgements We would like to thank David Kohlstedt at the University of Minnesota for kindly allowing us to use the facilities in his laboratory. We would also like to thank David Bruhn for helpful discussions in the early stages of the project. Peter McSwiggen provided help in determining the composition of our samples and in providing some SEM images. This research was supported by the National Science Foundation through grant EAR-9805217.

References

Ando K, Oishi Y (1974) Self-diffusion coefficients of oxygen ion in single crystals of MgO–nAl_2O_3 spinels. J Chem Phys 61: 625–629

Ashby MF, Verrall RA (1973) Diffusion accommodated flow and superplasticity. Acta Metall 21: 149–163

Bai Q, Green HW II (1998) Plastic flow of Mn_2GeO_4 I: toward a rheological model of the Earth's transition zone. In: Manghnani MH, Yagi T (eds) Properties of Earth and planetary materials at high pressure and temperature, Geophys Mon Ser, AGU, Washington, DC, 101: 461–472

Boy JH, Wirtz GP (1994) Grain boundary modifications of manganese ferrites. J Eur Ceram Soc 14: 227–235

Bretheau T, Castaing J, Rabier J, Veyssière P (1979) Dislocation motion and high temperature plasticity of binary and ternary oxides (in French). Adv Phys 28: 829–1014

Cannon WR, Langdon TG (1988) Creep of ceramics, part 2. An examination of flow mechanisms. J Mater Sci 23: 1–20

Chiang Y, Kingery W (1990) Grain-boundary migration in nonstoichiometric solid solutions of magnesium aluminate spinel: part 2. Effects of grain boundary nonstoichiometry. J Am Ceram Soc 73: 1153–1158

Chopra PN, Paterson MS (1984) The role of water in the deformation of dunite. J Geophys Res 89: 7861–7876

Doukhan N, Duclos R, Escaig B (1976) Influence of the stoichiometry on the mechanical properties of spinel $MgO{\cdot}n(Al_2O_3)$ single crystals. J Phys (C)7: 566–571

Doukhan N, Duclos R, Escaig B (1979) Sessile dissociation in the stoichiometric spinel $MgAl_2O_4$. J Phys 40: 381–387

Duclos R (1981) High-temperature deformation of $MgO{\cdot}1.8Al_2O_3$ spinel single crystals of $\langle 1\,1\,1 \rangle$ axial orientation. J Phys (C)3: 49–58

Duclos R, Doukhan N, Escaig B (1978) High-temperature creep behavior of nearly stoichiometric alumina spinel. J Mater Sci 13:1740–1748

Dupas-Bruzek C, Tingle T, Green HW II, Doukhan N, Doukhan JC (1998) The rheology of olivine and spinel magnesium germanate (Mg_2GeO_4): TEM study of the defect microstructures. Phys Chem Miner 25: 501–514

Frost HJ, Ashby MF (1982) Deformation-mechanism maps. Pergamon Press, Oxford, 166 pp

Gifkins RC (1978) Grain rearrangements during superplastic deformation. J Mater Sci 13: 1926–1936

Green HW II, Burnley PC (1989) A new self-organizing mechanism for deep-focus earthquakes. Nature 341: 733–737

Greskovich C, Schmalzried H (1970) Nonstoichiometry and electronic defects in Co_2SiO_4 and in $CoAl_2O_4$–$MgAl_2O_4$ crystalline solutions. J Phys Chem Solids 31: 639–646

Hwang L, Heuer AH, Mitchell TE (1975) Slip systems in stoichiometric $MgAl_2O_4$ spinel. In: Bradt RC, Tressler TE (eds) Deformation of ceramics. Plenum Press, New York, pp 257–270

Karato S (1989) Plasticity-crystal structure systematics in dense oxides and its implications for the creep strength of the Earth's deep interior: a preliminary result. Phys Earth Planet Int 55: 234–240

Karato S Rubie DC (1997) Toward an experimental study of deep mantle rheology: a new multianvil sample assembly for deformation studies under high pressures and temperatures. J Geophys Res 102: 20,111–20,122

Karato S, Paterson MS, FitzGerald JD (1986) Rheology of synthetic olivine aggregates: influence of grain size and water. J Geophys Res (B)91: 8151–8176

Karato S, Wang Z, Liu B, Fujino K (1995) Plastic deformation of garnets: systematics and implications for the rheology of the mantle transition zone. Earth Planet Sci Lett 130: 13–30

Karato S, Dupas-Bruzek C, Rubie D (1998) Plastic deformation of $(Mg,Fe)_2SiO_4$ spinel (ringwoodite) under the transition zone conditions of the Earth's mantle. Nature 395: 266–269

Karato S, Riedel MR, Yuen DA (2000) Rheological structure and deformation of subducted slabs in the mantle transition zone: implications for mantle circulation and deep earthquakes. Phys Earth Planet Int (in press)

Kizhappili R, Karato S (1996) Diffusion creep in Mg_2GeO_4 olivine. EOS Trans 77: F715–716

Lindner R, Åkerström Å (1958) Diffusion of Ni^{63} in nickel spinels. Z Phys Chem (Frankfurt) 18: 303–307

Mitchell T, Hwang L, Heuer A (1976) Deformation in spinel. J Mater Sci 11: 264–272

Nabarro FRN (1967) Steady-state diffusional creep. Phil Mag 16: 231–237

Navrotsky A (1967) The thermodynamics of cation distributions in simple spinels. J Inorg Chem 29: 2701–2714

Navrotsky A (1973) Thermodynamic relations among olivine, spinel and phenacite structures in silicates and germanates: I. Volume relations and the systems NiO–MgO–GeO_2 and CoO–MgO–GeO_2. J Solid State Chem 6: 21–41

Navrotsky A (1977) Calculation of effect of cation disorder on silicate spinel phase boundaries. Earth Planet Sci Lett 33: 437–442

Navrotsky A, Hughes L Jr. (1976) Thermodynamic relations among olivine, spinel, and phenacite structures in silicates and germanates. V. The system MgO–FeO–GeO_2. J Solid State Chem 16: 185–188

Navrotsky A, Kleppa OJ (1968) Thermodynamics of formation of simple spinels. J Inorg Chem 30: 479–498

Nishikawa T, Okamoto Y, Nakagawa T, Kimura H (1979) Diffusional creep of polycrystalline Ni–Zn ferrite of coarse grain. Yogyo-Kyokai-Shi (Japanese) 87: 529–536

Nishikawa T, Okamoto Y, Nakagawa T, Kimura H, Takeda H (1980) Dislocation climb-controlled creep of polycrystalline Mn–Zn ferrite. Yogyo-Kyokai-Shi (Japanese) 88: 538–546

O'Bryan H Jr, Dimarcello F (1970) Oxygen diffusion in nickel ferrous ferrite. J Am Ceram Soc 53: 413–416

Ogawa S, Nakajima T, Sasaki T, Takahashi M (1968) Ion diffusion and disaccommodation in ferrites. Jpne J Appl Phys 7: 899–903

Okamoto Y (1989) Creep deformation mechanisms in oxides and deformation of spinel ferrites. In: Karato S (ed) Rheology of solids and of the Earth. Oxford University Press, pp 83–104

Panda PC, Raj R (1985) Superplastic deformation in fine-grained $MgO{\cdot}2Al_2O_3$ spinel. J Am Ceram Soc 68: 522–529

Paterson MS (1990) Rock deformation experiments. In: Duba AG, Durham WB, Handin JW, Wang HF (eds) The brittle-ductile transition in rocks, The Heard volume. Geophys Mon Ser. AGU, Washington, DC, 56: 187–194

Raj R, Ashby MF (1971) On grain boundary sliding and diffusion creep. Trans Metall Soc AIME 2: 1113–1127

Ricoult DL, Kohlstedt DL (1985) Creep of Fe_2SiO_4 and Co_2SiO_4 single crystals in controlled thermodynamic environments. Philos Mag (A)51: 79–93

Ringwood AE (1970) Phase transformations and the constitution of the mantle. Phys Earth Planet Int 3: 109–155

Vaughan P, Coe R (1981) Creep mechanism in Mg_2GeO_4: effect of a phase transition. J Geophys Res 86: 389–404

Veyssière P, Rabier J, Garem H, Grilhé J (1978) Influence of temperature on dissociation of dislocations and plastic deformation in spinel oxides. Philos Mag A38: 61–79

Weertman J (1968) Dislocation climb theory of steady-state creep. Trans ASM 61: 681–694

Wolfenstine J, Kohlstedt DL (1994) High-temperature creep and kinetic decomposition of Ni_2SiO_4. Phys Chem Miner 21: 234–243